Exchange field effect in the crystal-field ground state of CeMAl_{4}Si_{2}

K. Chen, F. Strigari, M. Sundermann, S. Agrestini, N. J. Ghimire, S.-Z. Lin, C. D. Batista, E. D. Bauer, J. D. Thompson, E. Otero, A. Tanaka, and A. Severing

Phys. Rev. B **94**, 115111 — Published 6 September 2016

DOI: 10.1103/PhysRevB.94.115111

Exchange field effect in the crystal-field ground state of CeMAl$_4$Si$_2$

K. Chen,[1] F. Strigari,[1] M. Sundermann,[1] S. Agrestini,[2] N. J. Ghimire,[3] S. -Z. Lin,[3]
C. D. Batista,[3,4] E. D. Bauer,[3] J. D. Thompson,[3] E. Otero,[5] A. Tanaka,[6] and A. Severing[1]

[1]*Institute of Physics II, University of Cologne, Zülpicher Straße 77, 50937 Cologne, Germany*
[2]*Max Planck Institute for Chemical Physics of Solids, Nöthnizer Straße 40, 01187 Dresden, Germany*
[3]*Los Alamos National Laboratory, Los Alamos, New Mexico 87545, USA*
[4]*Department of Physics and Astronomy, The University of Tennessee, Knoxville, Tennessee 37996, USA*
[5]*Synchrotron SOLEIL, L'Orme des Merisiers, Saint-Aubin, 91192 Gif-sur-Yvette, France*
[6]*Department of Quantum Matter, AdSM, Hiroshima University, Higashi-Hiroshima 739-8530, Japan*

(Dated: August 1, 2016)

The crystal-field ground state wave functions of the tetragonal, magnetically ordering Kondo lattice materials CeMAl$_4$Si$_2$ (M = Rh, Ir and Pt) are determined with low-temperature linearly polarized soft x-ray absorption spectroscopy, and estimates for the crystal-field splittings are given from the temperature evolution of the linear dichroism. Values for the dominant exchange field in the magnetically ordered phases can be obtained from fitting the influence of magnetic order on the linear dichroism. The direction of the required exchange field is $\| c$ for the antiferromagnetic Rh and Ir compounds, with the corresponding strength of the order of $\lambda_{ex} \approx 6$meV (65K). Furthermore the presence of Kondo screening in the Rh and Ir compound is demonstrated on the basis of the absorption due to f^0 in the initial state.

The tetragonal cerium families CeM_2Si$_2$ and CeMIn$_5$ (or more generally Ce$_m M_n$In$_{3m+2n}$, where m and n are the number of the CeIn$_3$ and MIn$_2$ building blocks) are prototypical heavy-fermion materials where the substitution of the transition element M or application of pressure may drive the system from a well localized and magnetically ordered state into a more itinerant, unconventional superconducting ground state. The systematic investigation of the above mentioned substitution series has contributed tremendously to the understanding of the underlying physical mechanisms in ground state formation. However, the proximity of magnetic order, in most cases antiferromagnetic, and superconductivity is still a fascinating and, despite great progress, not fully understood puzzle in modern solid state physics.[1–8]

It is accepted that in Ce based compounds the hybridization of f and conduction electrons (cf-hybridization) leads to the competition of the indirect Ruderman-Kittel-Kasya-Yosida (RKKY) interaction and the on-site Kondo interaction. This competition has a great impact on ground state formation which is illustrated in the Doniach phase diagram,[9] where the exchange interaction J_{ex} can be tuned by different control parameters like doping, pressure, or magnetic field. For small exchange interactions the RKKY interaction forms a magnetically ordered ground state. With increasing J_{ex} the RKKY interaction increases at first before magnetic order is suppressed by the dominance of Kondo interaction. The latter leads to a screening of the local magnetic moments resulting in a non-magnetic singlet ground state. Quantum critical points (QCP) and unconventional superconductivity have been reported when going from one regime to the other.[10–12] More recent calculations suggest that the dimensionality of the system can be used to control the type of QCP[13,14] and lowering the dimensionality is believed to result in an increase of the superconducting transition temperature.[15] This calls for new classes of f-electron materials in which the dimensionality can be systematically tuned.

Here the members of the tetragonal CeM_nAl$_{2n+1}$Si$_2$ family with tunable dimensionality comes into focus, in particular the recently synthesized $n = 1$ members, namely CeMAl$_4$Si$_2$ with M = Rh, Ir, and Pt.[16,17] According to susceptibility measurements CeRhAl$_4$Si$_2$ and CeIrAl$_4$Si$_2$ order antiferromagnetically with two magnetic transitions at $T_{N1} = 14$K and $T_{N2} = 9$ K and at $T_{N1} = 16$K and $T_{N2} = 14$ K, respectively and ordered moments aligned along the c axis while CePtAl$_4$Si$_2$ becomes ferromagnetic at $T_C = 3$ K with the moments aligned in the basal plane. Neutron diffraction and Al^{27} NMR studies of the Rh and Ir samples confirm this; below T$_{N2}$ the magnetic order is commensurate and the moments are aligned in ferromagnetic planes in antiferromagnetic stacking along the c axis.[18,19] Between T_{N1} and T_{N2} the magnetic order is incommensurate.[19,20] The ordered magnetic moments are much smaller than the full moment of the $J = 5/2$ Hund's rule ground state and the magnetic and transport data are strongly anisotropic, both suggesting the presence of crystalline-electric field (CEF) effects. In addition, Maurya *et al.* suggest that Kondo screening reduces the magnetic moments further.[17]

The goal of the present work is to determine the CEF potential of CeMAl$_4$Si$_2$ with M = Rh, Ir, and Pt. The CEF ground state wave functions are investigated by analysis of the low-temperature linearly polarized soft x-ray absorption spectroscopy (XAS) data at the Ce^{3+} (f^1) M-edge and the CEF splittings are determined from the temperature-dependent linear dichroism (LD). For Rh and Ir samples, at low temperatures close to the magnetically ordered phases ($T < 20$ K) a further change in LD has been observed that cannot be accounted for by population of excited CEF states. It turns out that this is due to the impact of the exchange interaction $H_{\rm ex}$, in

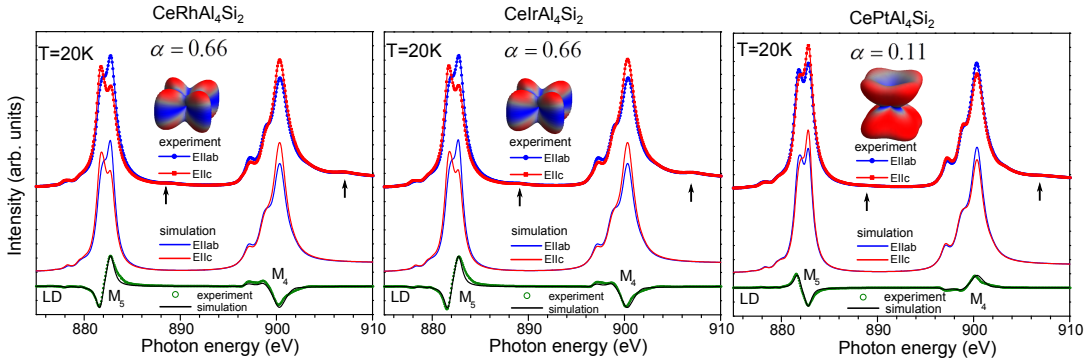

FIG. 1. Experimental low-temperature (T = 20 K) linearly polarized soft x-ray data of $CeRhAl_4Si_2$ (left), $CeIrAl_4Si_2$ (middle) and $CePtAl_4Si_2$ (right) at the Ce $M_{4,5}$ absorption edge. At the top of each panel the experimental data and in the middle the simulations are shown. The green circles and black lines at the bottom represent the corresponding experimental and simulated linear dichroism, respectively, and the corresponding spatial distributions of the $4f$ electrons are included as insets. The black arrows indicate the position of absorption due to f^0 in the initial state.

addition to the CEF potential ($H_{\rm CEF}$). An estimate for the most important exchange field will be given. With increasing cf-hybridization the f-electrons tend to delocalize increasingly so that the ground state becomes a mixed state with some small amount of Ce^{4+} (f^0). The amount of absorption due to the f^0 contribution in the initial state allows us to order the three compounds qualitatively according to their exchange interaction.

High-quality single crystals of $CeMAl_4Si_2$ (M = Rh, Ir, Pt) were grown out of Al/Si eutectic flux.[16] $CeMAl_4Si_2$ crystallizes in the KCu_4S_3-type tetragonal lattice structure (space group $P4/mmm$) with lattice parameters of $a = b = 4.227$, 4.233, and 4.271 Å, and $c = 8.047$, 8.035, and 8.060 Å for M = Rh, Ir and Pt, respectively. The sequential stacking of $BaAl_4$-type Ce containing layers separated by MAl_2 slabs along the c-axis. The Ce-Ce distance in the ab-plane is ≈ 4.2 Å and ≈ 8 Å along the c axis, albeit separated by the MAl_2 slab. More details of the crystal structure and sample characterization can be found in Refs. [16,18]. XAS and LD spectra at the Ce $M_{4,5}$ edges were measured at temperatures from 4 to 300 K at the DEIMOS beamline[21] in the synchrotron facility SOLEIL. The spectra were recorded for $E \perp c$ and $E \parallel c$, E is the polarization vector of the soft x-ray. The LD is defined as the differences of the absorption intensities $I_{E\perp c} - I_{E\parallel c}$.[22] Clean sample surfaces were obtained by cleaving the samples *in situ* in the *ac* plane under ultra high vacuum (UHV). All spectra were recorded in the total electron yield (TEY) mode in the UHV chamber with a pressure in the 10^{-10} mbar range. The energy resolution at the Ce $M_{4,5}$ edges ($h\nu \approx 875-910$ eV) was set to 0.10 eV.

The XAS data were simulated with ionic full multiplet calculations which include Coulomb (H_C) and spin orbit interaction (H_{SO}) using the XTLS 8.3 program.[23] All atomic parameters are given by Hartree-Fock values, with a reduction of about 40 % for the $4f-4f$ Coulomb exchange interactions and of about 20 % for the $3d-4f$ interactions. These reduction factors account for the configuration interaction effects not included in the Hartree-Fock scheme and compare well with our findings for other cerium compounds.[24–26] Once the atomic parameters were fine-tuned to reproduce best the isotropic spectra ($I_{\rm isotropic} = 2I_{E\perp c} + I_{E\parallel c}$), the polarization dependence in XAS was solely described by the crystal-field Hamiltonian H_{CEF} for the tetragonal crystal-electric field.

Figure 1 shows the polarization-dependent XAS data of $CeRhAl_4Si_2$, $CeIrAl_4Si_2$ and $CePtAl_4Si_2$ at the Ce $M_{4,5}$ absorption edge. The main absorption is due to the transition $3d^{10}f^1 \rightarrow 3d^9f^2$ and only a small amount is due to $3d^{10}f^0 \rightarrow 3d^9f^1$ (see black arrows in Fig. 1). The data were taken at 20 K which is sufficiently low to guarantee that only the ground state is probed since according to macroscopic data the first excited CEF level is expected to be at about 100 K in these compounds.[16] The polarization of the M = Rh and Ir data look very much alike suggesting similar ground-state wave functions, whereas that of the Pt sample has an opposite polarization. Because of the tetragonal symmetry the probed state is either a $\Gamma_6 = |\pm 1/2\rangle$ or one of the two mixed states $\Gamma_7^1 = \alpha|\pm 5/2\rangle \pm \sqrt{1-\alpha^2}\ |\mp 3/2\rangle$ or $\Gamma_7^2 = \sqrt{1-\alpha^2}|\pm 5/2\rangle \mp \alpha\ |\mp 3/2\rangle$. In case of a mixed state, the mixing parameter α needs to be determined.

Comparision of the data and the simulations of the pure states (see Refs. [24] and [25]) excludes the $|J_z\rangle = |\pm 1/2\rangle$ as ground state, and the *map* of the polarization changes of α between 0 and 1 as presented in Ref. [24] shows that all three compounds have a Γ_7-type ground state. This analysis further shows the $|J_z\rangle = |\pm 3/2\rangle$ contribution is largest in the Pt compound. The fitting yields

$$CeRhAl_4Si_2\text{: } |0\rangle = 0.66|\pm 5/2\rangle \pm 0.75|\mp 3/2\rangle \quad (1)$$

$$CeIrAl_4Si_2\text{: } |0\rangle = 0.66|\pm 5/2\rangle \pm 0.75|\mp 3/2\rangle \quad (2)$$

$$CePtAl_4Si_2\text{: } |0\rangle = 0.12|\pm 5/2\rangle \pm 0.99|\mp 3/2\rangle \quad (3)$$

as ground-state wave functions with an accuracy of $\Delta\alpha = \pm 0.02$. The simulations of the $M_{4,5}$ edges are

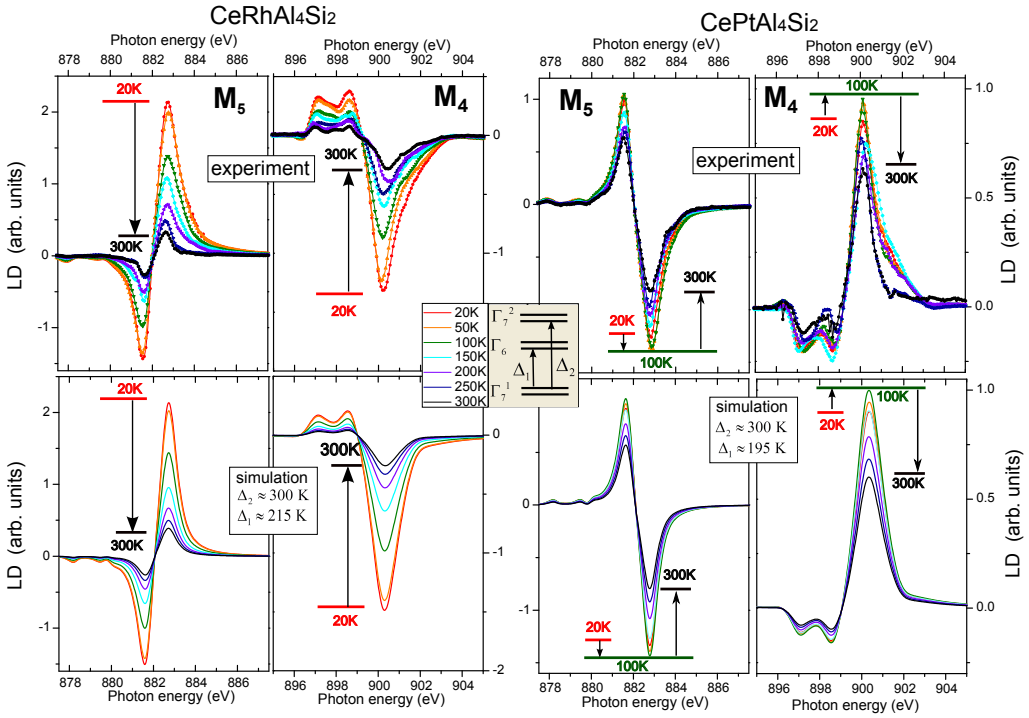

FIG. 2. Temperature-dependent (20 - 300 K) linear dichroism of the Ce^{3+} $M_{4,5}$ edge of $CeRhAl_4Si_2$ (left panel) and $CePtAl_4Si_2$ (right panel). The experimental data are shown in the upper part of each panel and the best fitting simulation of the LD spectra are given in the lower part. The sequence of crystal-field states is shown as inset.

shown in the middle of each panel of Fig. 1. The measured and simulated LD presented on the bottom of each panel in Fig. 1 are in perfect agreement. Inset in each panel shows the corresponding spatial distributions of the $4f$ electrons. The two antiferromagnetic compounds with ordered moments along c have oblate ground state f orbitals in contrast to ferromagnetic $CePtAl_4Ai_2$ with ordered moments in the basal plane which has a prolate ground state orbital.

Temperature dependence of the measured and simulated LDs of both absorption edges (Ce M_5 and M_4) for temperatures between 20 and 300 K are presneted in Fig. 2. Temperature dependence of the polarization arises due to thermal population of excited states, i.e. at elevated temperature the superposition of the polarizations of each thermally excited state is measured. The polarization dependence (LD) should vanish when all crystal-field states are equally populated because this situation reflects the isotropic, *non* crystal-field split Hund's rule ground state. The top panels show the measured LD of $CeRhAl_4Si_2$ and $CePtAl_4Si_2$. The temperature-dependent LD spectra of $CeIrAl_4Si_2$ are quite similar to those of $CeRhAl_4Si_2$ and therefore not shown. For $CeRhAl_4Si_2$ the LD decreases successively with increasing temperature, whereas in the Pt compound it increases at first up to 50 - 100 K before it also decreases with further rising temperature. For all three compounds, such a temperature dependence can only be explained with a Γ_6 as first excited and a Γ_7^2 as second excited state (cf. discussion of temperature dependence of $CePt_3Si$ in Ref. [25]).

Knowing the sequence of states from the above consideration allows us to simulate the temperature dependence by fitting the CEF transition energies to a successively populating three level system. The bottom of Fig. 2 shows the best fit to the temperature dependence of the respective LDs. We find the first excited CEF energy $(\Delta_1) \cong 215 \pm 10$ K for $CeRhAl_4Si_2$ ($CeIrAl_4Si_2$) and $\cong 195 \pm 10$ K for $CePtAl_4Si_2$. The second excited state $(\Delta_2) \cong 300 \pm 15$ K.[27] The values of the in-plane ($g_\parallel$) and out-of-plane ($g_\perp$) components of the g factor can be calculated based on the ground states: $g_\parallel = g_L(8\alpha^2 - 3)$, $g_\perp = g_L(2\sqrt{5}\alpha\sqrt{1-\alpha^2})$, with the Lande g-factor g_J of 6/7 for Ce^{3+}. Using the α value determined above, we obtain the g factor as: $g_\parallel = 0.41$, $g_\perp = 1.90$ for $CeRhAl_4Si_2$ and $CeIrAl_4Si_2$ samples, and $g_\parallel = 2.47, g_\perp = 0.46$ for $CePtAl_4Si_2$.

Above 20 K the polarization-dependent spectra and the temperature dependence of the LD are well described with the CEF scheme described above. Such a CEF scheme with levels at 200 and 300 K will not give rise to any T-dependence between $T = 4$ and 20 K since at such low temperatures thermal population has no impact. Interestingly, when comparing the data at $T = 4$ K and 20 K [see dotted lines Fig. 3 (a)] there is a small but clear enhancement of the LD in $CeRhAl_4Si_2$ ($CeIrAl_4Si_2$). The deviation of a CEF-only model from the true temperature dependence of the LD can be seen clearly in Fig. 3 (c),

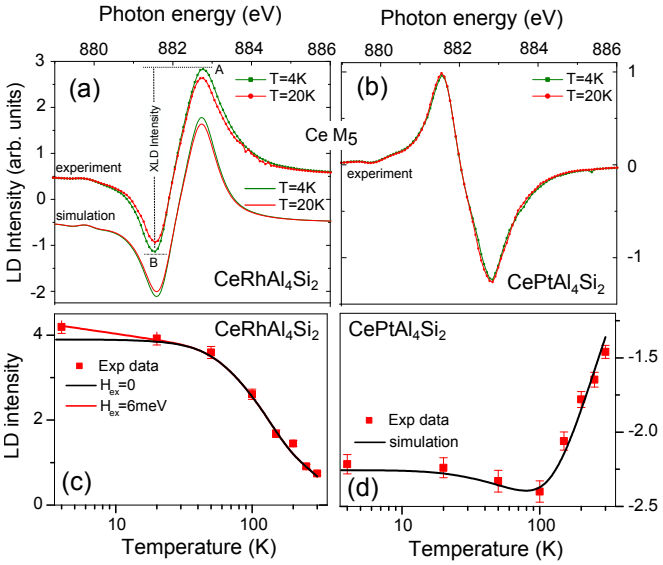

FIG. 3. Influence of the exchange field on the LD intensity. (a)Experimental LD spectra at 4 and 20 K and simulations with exchange field for $CeRhAl_4Si_2$. $H_{ex} \parallel [0,0,1] \cong 6$ meV are used in the simulations for $CeRhAl_4Si_2$. (b)Experimental LD spectra at 4 and 20 K for $CePtAl_4Si_2$. (c)Temperature-dependent LD intensity, with and without exchange field, for $CeRhAl_4Si_2$. The LD intensity is modified at $T < 20$ K when an exchange field is considered. (d)Temperature-dependent LD intensity of $CePtAl_4Si_2$ can be well fitted at $T < 20$ K without the exchange field.

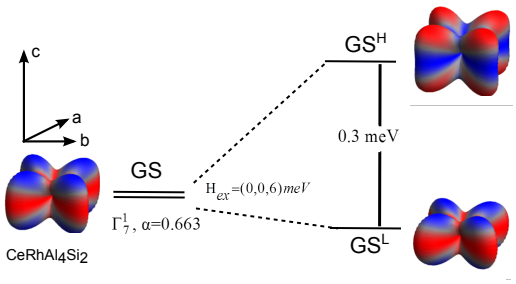

FIG. 4. Impact of an exchange field on the CEF ground state. For $CeRhAl_4Si_2$ the Zeeman splitting of the ground-state doublet amounts to 0.3 meV, when an exchange field field $H_{ex} \parallel [0,0,1] \cong 6$ meV is active at 4 K. The $J_z = |\pm 5/2\rangle$ contribution is enhanced in the lower singlet with respect to $H_{ex} = 0$.

where the difference of maximum and minimum LD [referred to as *LD intensity* in Fig. 3 (a)] as function of temperature is compared with the CEF-only simulation (black line). The discrepancy is observed in the magnetically ordered phase of $CeRhAl_4Si_2$ ($CeIrAl_4Si_2$) but not for $CePtAl_4Si_2$ where all data were taken above the ordering transition temperature. It is therefore appropriate to use an exchange field to account for the deviation from the CEF-only LD and we apply the following Hamiltonian

$$H = H_C + H_{SO} + H_{\mathrm{CEF}} + H_{\mathrm{ex}} \qquad (4)$$

for the magnetically ordered phase of the Rh and Ir compounds. Here the the exchange interaction H_{ex} acts on the ion in addition to Coulomb, spin orbit and CEF interaction. H_{ex} leads to a Zeeman splitting of the Kramers' doublets and a reshuffling of the J_z contributions via the excited states and consequently a change in LD. We find that below 20 K an exchange field $\parallel c$ ($H_{\mathrm{ex}} \parallel [0,0,1] \cong 6$ meV) is required to describes the LD well (see red line in Fig. 3 (c)). The resulting Zeeman splitting of the ground state Kramers doublets is shown in Fig. 4. The $J_z = |\pm 5/2\rangle$ contribution in the lower singlet GS^L is enhanced so that the LD increases with respect to $H_{\mathrm{ex}} = 0$ at 20 K. In principle we expect that the two levels of a Zeeman split Kramers doublet are identical and that the LD remains unchanged. However, it turns out the exchange/Zeeman split CEF states of the same irreducible representation mix with one another when the exchange/Zeeman splitting is large enough with respect to the CEF splitting. As a result the J_z admixtures in the magnetically ordered phase are slightly modified (reshuffled) with respect to the paramagnetic phase and the LDs differ accordingly. Note, the Boltzmann occupation of the higher Zeeman split states have to be taken into account when calculating the size of the LD. The effect is therefore small. Also most measurements for CEF purposes are performed well above the ordering transitions (see e.g. Ref.s 28–31)so that this effect us usually not observed.

The different CEF ground state wave function of the Pt compound with respect to Rh (Ir) reflects the different magnetic behavior within the $CeMAl_4Si_2$ family and our CEF models reproduce the anisotropy of the high temperature susceptibilities. As shown in Fig. 5, the magnetic susceptibility along the easy axis is well described with the CEF-only calculation, however, along the hard axis, a better description requires additional anisotropic molecular field λ, which are $\lambda_{ab} = -60$ and $\lambda_c = -80$ mol-f.u./emu for $CeRhAl_4Si_2$ and $CePtAl_4Si_2$, respectively. At low temperatures deviation between the experimental and CEF-only calculation are observed along the easy axis in both materials. It indicates that magnetic correlations other than the CEF effect start to dominate the magnetic anisotropy. The antiferromagnetic spin structures of Rh and Ir compounds (with spins parallel or antiparallel to the c axis) determined from neutron diffraction[16,19] require a strong exchange field $\parallel c$ at low temperature, which is confirmed by our results. The CEF-only magnetic moments which are calculated at 20 K for an infinitesimal small field (∼0.1Oe) amount to $0.95\,\mu_B/\mathrm{Ce} \perp c$ ($M = $ Rh, Ir) and $1.18\,\mu_B/\mathrm{Ce} \parallel c$ ($M = $ Pt), respectively, i.e. they agree well in size with findings from magnetization but at low T the anisotropy is not reproduced by the CEF-only simulation, thus stressing again the impact of the exchange fields.

We provide an estimate of the exchange field H_{ex} in

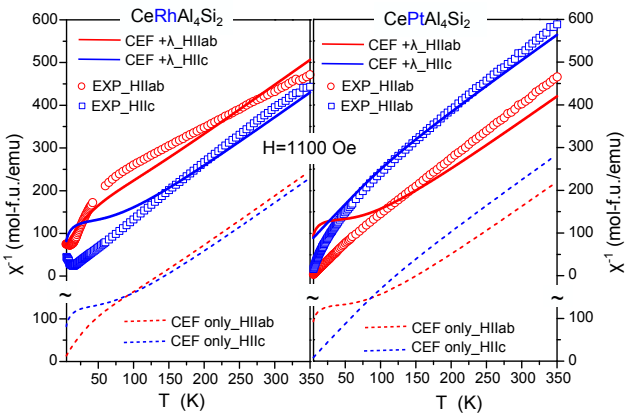

FIG. 5. χ^{-1} of $CeRhAl_4Si_2$ and $CePtAl_4Si_2$, compared to the results from CEF. At high temperature the magnetic anisotropy canbe reproduced from the CEF-only calculation, however, a better description requires addtional anisotropic molecular field λ along the hard axis, which are $\lambda_{ab} = -60$ and $\lambda_c = -80$ mol-f.u./emu for $CeRhAl_4Si_2$ and $CePtAl_4Si_2$, respectively.

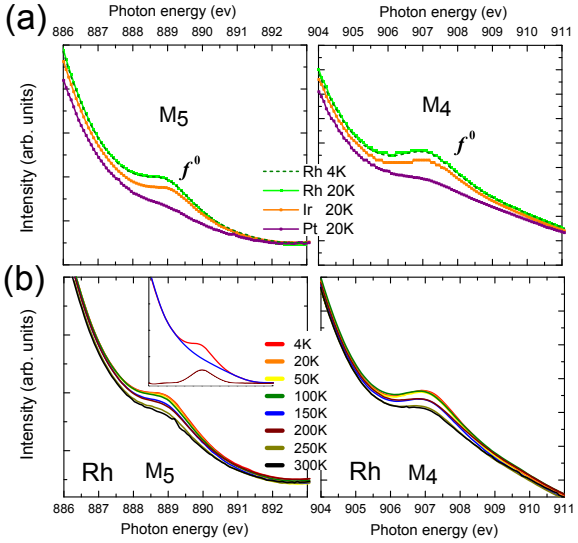

FIG. 6. (a)Isotropic spectra of $CeMAl_4Si_2$ for the absorption due to f^0 in the ground state and (b) M = Rh f^0 spectral weight for all temperatures. The isotropic spectra are constructed from the polarized data and normalized to the total (f^1 and f^0) integrated absorption intensity.

the ordered state for M=Rh and Ir based compounds on the available experimental data presented here and in Refs. 16, 17, and 19. A detailed theoretical model that reproduces the magnetic phase diagram of $CeMAl_4Si_2$ will be published elsewhere.[32] The interaction between the Ce ions is of RKKY type and the Hamiltonian is given by $\mathcal{H} = -\sum_{\mu=a,b,c}\int dq^3 J(\mathbf{q}) a_\mu S_\mu(\mathbf{q}) S_\mu(-\mathbf{q})/2$, where $J(\mathbf{q})$ is the RKKY interaction, $S(\mathbf{q})$ is the magnetic moment in the momentum space and $\boldsymbol{a} = (\eta, \eta, 1)$ accounts for the uniaxial anisotropy. For M=Rh, Ir there is a strong easy axis anisotropy along the c direction: $\eta \gg 1$. For M=Pt, the anisotropy is of the easy-plane type: $\eta < 1$. For $\eta \gg 1$, the mean field value of the ordering temperature, T_{N1}, is given by $T_{N1}^{MF} = J_c(\mathbf{Q}_o)S^2$, where $\mathbf{Q}_o$ is the optimal ordering wavevector that maximizes $J_c(\mathbf{q})$. According to the neutron scattering measurement, we know that $\mathbf{Q}_o \approx (0.02, 0.02, 0.5)$ at T_{N1} for M=Rh and Ir.[19] The exchange field $H_{\rm ex}$ below T_{N1} is $H_{\rm ex} = J_c(\mathbf{Q})\langle S\rangle^2$ where $\langle S\rangle$ is the thermally averaged magnetic moment, and $\mathbf{Q}$ is the ordering wave vector at a given temperature ($\mathbf{Q} = \mathbf{Q}_o$ at $T = T_{N1}$). Because $\mathbf{Q}$ remains close to $\mathbf{Q}_o$ at any temperature, we approximate $J_c(\mathbf{Q})$ by $J_c(\mathbf{Q}_o)$. In addition, we have that $\langle S\rangle \approx S$ for $T \ll T_{N1}$.

The mean field analysis then identifies the exchange field with mean field ordering temperature: $H_{\rm ex} \approx T_{N1}^{MF}$. However, it is known that the actual ordering temperature is significantly lower than the mean field estimate, $T_{N1} < T_{N1}^{MF}$, due to the effect of thermal fluctuations, which are neglected in the mean field analysis. For instance, according to Onsager's solution,[33] $T_c^{MF} \simeq 2\ln(1+\sqrt{2})T_c$ for a two-dimensional ferromagnetic Ising model. This ratio increases upon including competing exchange interactions (frustration), which enhance the effect of the thermal fluctuations. It can be shown that the same competing interactions that induce the observed incommensurate orderings in $CeMAl_4Si_2$ with M=Rh and Ir, can also enhance the T_{N1}^{MF}/T_{N1} ratio to values between 3 and 4,[32] in agreement with the LD data for these compounds.

Finally, we compare the regions of absorption for the transitions from the $3d^{10}4f^0$ initial state for the 20 K data (see black arrows in Fig. 1). These regions are shown for the isotropic data on an enlarged scale in Fig. 5. For the Rh and Ir compounds (light green and orange lines) the humps are fairly pronounced while they are barely visible for the ferromagnetic Pt sample (purple line). We can further state that the f^0 contributions are unaffected by the magnetic order by comparing with the 4 K data (see thin dark green lines) which fall on top of the 20 K data. Warming up to 300 K reduces the f^0 spectral weight as expected when depopulating the Kondo singlet state. However, here the temperature dependence of the f^0 spectral weight does not appear to be well suited for determining the Kondo temperature since excited CEF states are becoming populated in the same temperature interval.

Qualitatively, the weak f^0 humps in the Pt sample and its lowest ordering temperature within the family give rise to the assumption that it is far to the left in the Doniach phase diagram, i.e. in the region of minor Kondo screening. The ferromagnetic ordering (in contrast to the antiferromagnetic ordering) despite having the largest Ce-Ce bond distance might be another indication for the weak exchange interaction in this compound. The presence of more pronounced f^0 humps in Rh and Ir compounds clearly show the presence of Kondo screening, which puts them closer to the maximum of the ordering

temperature in the Doniach diagram – in line with the reasoning presented in Ref. 16 on the basis of the fairly high ordering temperatures. This makes the latter two compounds ideal candidates for becoming quantum critical and/or superconducting under applied pressure, making the $CeMAl_4Si_2$ another model family for investigating the interplay of magnetism and superconductivity.

To summarize, the CEF ground state wave functions of the Kondo lattice $CeMAl_4Si_2$ (M = Rh, Ir and Pt) single crystals have been determined with low-temperature linearly polarized soft XAS and the CEF splitting energies were obtained from the temperature dependence of the linear dichroism intensity. Furthermore, the impact of the exchange field in the magnetically ordered state has been detected and an estimate for the dominant exchange fields acting on the Ce ions in $CeMAl_4Si_2$ (M = Rh and Ir) are given. The f^0 contribution in the ground states of the Rh and Ir compounds points towards the presence of Kondo screening, making them ideal candidates for further investigations.

K.C., F.S., M.S. and A.S. benefited from support of the German funding agency DFG (Project 615811). We further acknowledge SOLEIL for provision of their synchrotron radiation facilities. Work at Los Alamos National Laboratory was performed under the auspices of the U.S. Department of Energy, Office of Basic Energy Sciences, Division of Materials Science and Engineering and was funded in part by the LANL Laboratory Research and Development program.

[1] F. Steglich, J. Aarts, C. D. Bredl, W. Lieke, D. Meschede, W. Franz, and H. Schäfer, Phys. Rev. Lett. **43**, 1892 (1979).
[2] D. Jaccard, K. Behnia, and J. Sierro, Phys. Lett. A. **163**, 475 (1992).
[3] N. D. Mathur, F. M. Grosche, S. R. Julian, I. R. Walker, D. M. Freye, R. K. W. Haselwimmer, and G. G. Lonzarich, Nature. **394**, 39 (1998).
[4] H. Hegger, C. Petrovic, E. G. Moshopoulou, M. F. Hundley, J. L. Sarrao, Z. Fisk, and J. D. Thompson, Phys. Rev. Lett. **84**, 4986 (2000).
[5] P. Monthoux, D. Pines, and G. G. Lonzarich, Nature **450**, 1177 (2007).
[6] C. Pfleiderer, Rev. Mod. Phys. **81**, 1551 (2009).
[7] O. Stockert, J. Arndt, E. Faulhaber, C. Geibel, H. S. Jeevan, S. Kirchner, M. Loewenhaupt, K. Schmalzl, W. Schmidt, Q. Si, and F. Steglich, Nat. Phys. **7**, 119 (2011).
[8] J. D. Thompson and Z. Fisk, J Phys Soc Jpn **81**, 011001 (2012).
[9] S. Doniach, Physica B & C **91**, 231 (1997).
[10] H. v. Löhneysen, A. Rosch, M. Vojta, and P. Wölfle, Rev. Mod. Phys. **79**, 1015 (2007).
[11] O. Stockert and F. Steglich, Ann. Rev. **2**, 79 (2011).
[12] P. Aynajian, E. H. da Silva Neto, A. Gyenis, R. E. Baumbach, J. D. Thompson, Z. Fisk, E. D. Bauer, and A. Yazdani, Nature **486**, 201 (2012).
[13] P. Coleman and A. Nevidomskyy, J. Low Temp. Phys. **161**, 182 (2010).
[14] Q. Si, J. H. Pixley, E. Nica, S. J. Yamamoto, P. Goswami, R. Yu, and S. Kirchner, J. Phys. Soc. Jpn **83**, 061005 (2014).
[15] P. Monthoux and G. G. Lonzarich, Phys. Rev. B **69**, 064517 (2004).
[16] N. J. Ghimire, F. Ronning, D. Williams, B. L. Scott, Y. Luo, J. D. Thompson, and E. D. Bauer, J. Physics: Condensed Matter **27**, 025601 (2015).
[17] A. Maurya, R. Kulkarni, A. Thamizhavel, D. Paudyal, and S. K. Dhar, Journal of the Physical Society of Japan **85**, 034720 (2016).
[18] N. J. Ghimire, S. Calder, M. Janoschek, and E. Bauer, Journal of Physics: Condensed Matter **27**, 245603 (2015).
[19] J. Gunasekera, L. Harriger, A. Dahal, A. Maurya, T. Heitmann, S. M. Disseler, A. Thamizhavel, S. Dhar, D. J. Singh, and D. K. Singh, Phys. Rev. B **93**, 155151 (2016).
[20] H. Sakai, T. Hattori, Y. Tokunaga, S. Kambe, N. J. Ghimire, F. Ronning, E. D. Bauer, and J. D. Thompson, Phys. Rev. B **93**, 014402 (2016).
[21] P. Ohresser, E. Otero, F. Choueikani, K. Chen, S. Stanescu, F. Deschamps, T. Moreno, F. Polack, B. Lagarde, J.-P. Daguerre, F. Marteau, F. Scheurer, L. Joly, J.-P. Kappler, M. B., O. Bunau, and P. Sainctavit, Rev. Sci. Instrum. **85**, 013106 (2014).
[22] Specifying the direction within the fourfold rotational invariant tetragonal plane is not necessary since the in-plane LD is zero in a dipole experiment.
[23] A. Tanaka and T. Jo, J. Phys. Soc. Jpn. **63**, 2788 (1994).
[24] P. Hansmann, A. Severing, Z. Hu, M. W. Haverkort, C. F. Chang, S. Klein, A. Tanaka, H. H. Hsieh, H.-J. Lin, C. T. Chen, B. Få k, P. Lejay, and L. H. Tjeng, Phys. Rev. Lett. **100**, 066405 (2008).
[25] T. Willers, B. Fåk, N. Hollmann, P. O. Körner, Z. Hu, A. Tanaka, D. Schmitz, M. Enderle, G. Lapertot, L. H. Tjeng, and A. Severing, Phys. Rev. B **80**, 115106 (2009).
[26] C. Praetorius, M. Zinner, P. Hansmann, M. W. Haverkort, and K. Fauth, Phys. Rev. B **93**, 165107 (2016).
[27] The Stevens parameters B_2^0=−0.1497, B_4^0=0.0206, and $|B_4^4|$=0.4810 meV for $CeRhAl_4Si_2$, and B_2^0=0.6842, B_4^0=0.0692, and $|B_4^4|$=0.1107 meV for $CePtAl_4Si_2$ will give the above energies and wave functions. Please note that in the present simulations a *full* multiplet calculation was used.
[28] T. Willers, F. Strigari, N. Hiraoka, Y. Q. Cai, M. W. Haverkort, K.-D. Tsuei, Y. F. Liao, S. Seiro, C. Geibel, F. Steglich, L. H. Tjeng, and A. Severing, Phys. Rev. Lett. **109**, 046401 (2012).
[29] T. Willers, Z. Hu, N. Hollmann, P. O. Körner, J. Gegner, T. Burnus, H. Fujiwara, A. Tanaka, D. Schmitz, H. H. Hsieh, H.-J. Lin, C. T. Chen, E. D. Bauer, J. L. Sarrao, E. Goremychkin, M. Koza, L. H. Tjeng, and A. Severing, Phys. Rev. B **81**, 195114 (2010).
[30] T. Willers, D. T. Adroja, B. D. Rainford, Z. Hu, N. Hollmann, P. O. Körner, Y.-Y. Chin, D. Schmitz, H. H. Hsieh, H.-J. Lin, C. T. Chen, E. D. Bauer, J. L. Sarrao, K. J. McClellan, D. Byler, C. Geibel, F. Steglich, H. Aoki, P. Lejay, A. Tanaka, L. H. Tjeng, and A. Severing, Phys. Rev. B

85, 035117 (2012).
[31] T. Willers, F. Strigari, Z. Hu, V. Sessi, N. B. Brookes, E. D. Bauer, J. L. Sarrao, J. D. Thompson, A. Tanaka, S. Wirth, L. H. Tjeng, and A. Severing, Proc. Nat. Acad. Sci **112**, 2384 (2015).
[32] S.-Z. Lin et al., to be published. (2016).
[33] L. Onsager, Phys. Rev. **65**, 117 (1944).